Engineering Weyl phases and nonlinear Hall effects in T_d-$MoTe_2$

Sobhit Singh,* Jinwoong Kim, Karin M. Rabe, and David Vanderbilt
Department of Physics and Astronomy, Rutgers University, Piscataway, New Jersey 08854-8019, USA

$MoTe_2$ has recently attracted much attention due to the observation of pressure-induced superconductivity, exotic topological phase transitions, and nonlinear quantum effects. However, there has been debate on the intriguing structural phase transitions among various observed phases of $MoTe_2$, and their connection to the underlying topological electronic properties. In this work, by means of density-functional theory (DFT+U) calculations, we describe the structural phase transition between the polar T_d and nonpolar 1T′ phases of $MoTe_2$ in reference to a hypothetical high-symmetry T_0 phase that exhibits higher-order topological features. In the T_d phase we obtain a total of 12 Weyl points, which can be created/annihilated, dynamically manipulated, and switched by tuning a polar phonon mode. We also report the existence of a tunable nonlinear Hall effect in T_d-$MoTe_2$, and propose possible ways to observe this effect in experiments. In particular, we identify a configuration in which a nonlinear surface response current is predicted. The potential technological applications of the tunable Weyl phase and the nonlinear Hall effect are discussed.

Owing to its intriguing structural and electronic phase transitions and novel technological applications, $MoTe_2$ remains in the active area of research [1–9]. Specifically, the experimentally tunable structural phase transition between the 1T′ and T_d-phases [10–12] allows for the exploitation of the topological electronic properties and the electronic phase transitions, yielding various novel quantum phenomena such as extremely large magnetoresistance [13–16], Berry-curvature-induced planar Hall effect [17], nonlinear anomalous Hall effect [18], quantum spin Hall effect [19], spin-photogalvanic effect [20], quantum nonlinear Hall effect [21], large spin Hall conductivity with high spin Hall angles [22], complex Fermiology [23–25], and tunable polar/phase domain walls in $MoTe_2$ [12]. Recent theoretical and experimental work has confirmed the existence of type-I and type-II Weyl fermions in T_d-$MoTe_2$, and reported topological quantum oscillations and pressure-enhanced superconductivity [7, 10, 23, 26–35]. However, the total number and location of Weyl fermions in $MoTe_2$ are still under debate [23–26, 29, 32, 36]. Strikingly, a higher-order topological phase has been predicted in 1T′-$MoTe_2$ [37–39].

Despite the recent advances in understanding the topological electronic properties of $MoTe_2$ [10, 23, 26–29, 31–37], the link between the higher-order topological phase (1T′) and the Weyl phase (T_d) remains elusive. Kim et al. theoretically showed that the interlayer coupling is pivotal in determining distinct structural phase transitions in $MoTe_2$ [4]. Recent experiments further confirm the essential role of interlayer shear modes in governing the T_d-1T′ phase transition in $MoTe_2$ [4, 40, 41]. Notably, controlled mechanical [10], optical [41], dimensional [42, 43], and temperature [7, 44] -driven T_d-1T′ phase transitions have been experimentally demonstrated. A centrosymmetric phase ($T_d{}^*$) with no Weyl nodes has also been recently observed at the T_d-1T′ phase boundary [45, 46]. We find that most of the reported theoretical and experimental studies mainly focus on the characterization of distinct phases of $MoTe_2$. A systematic connection among these phases, in the context of the potential energy surface profile and crystal symmetries, has not been clarified in the literature.

In this work, by means of *ab-initio* density-functional theory (DFT) calculations, we first describe the intriguing structural phase transition between the polar T_d and nonpolar 1T′ phases of $MoTe_2$ by defining a high-symmetry reference phase T_0, which has a higher-order topological nature. We then study the evolution of the Weyl fermions in the polar phase along the polarity reversal path. We find that additional Weyl points (WPs) get created/annihilated *via* pair creation/annihilation process as we tune the spatial-inversion symmetry breaking parameter (λ). The WPs switch their chirality as we go from one to another polar variant of the T_d phase. Since this structural phase transition has recently been experimentally realized using electron beams [12], and notably, is completely reversible, we believe that the switching and pairwise creation/annihilation of Weyl fermions can be experimentally accessed in $MoTe_2$. We further demonstrate that a higher-order topological phase naturally appears when all WPs annihilate each other at $\lambda = 0$. Finally, we report on the existence of a tunable nonlinear Hall effect and discuss the role of dimensionality on this effect. We notice that the surface termination along the (001) direction leads to the manifestation of a nonlinear surface response current solely arising due to the broken symmetries at the surface. Such a tunable nonlinear Hall effect could lead to electrically switchable circular photogalvanic [20, 47], bulk rectification [48], and chiral polaritonic effects [49].

$MoTe_2$ crystallizes in three distinct phases: (i) 2H (hexagonal, space group $P6_3/mmc$), (ii) 1T′ (monoclinic, space group $P2_1/m$), and (iii) T_d (orthorhombic, space group $Pnm2_1$) [3, 4, 10, 40, 44, 50–52]. In all three phases, Mo and Te atoms form Te-Mo-Te triple layers, which stack along the *c*-axis and interact *via* weak van der Waals interactions. The Te atoms form symmetrical octahedra in the hexagonal 2H phase, whereas these octahe-

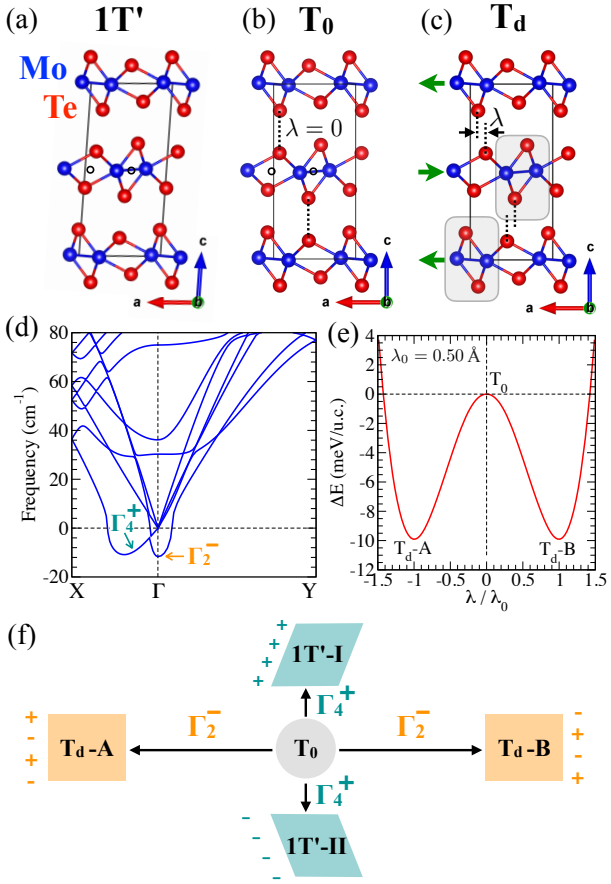

FIG. 1. Crystal structure of $MoTe_2$ in (a) 1T′, (b) designed T_0, and (c) T_d phases. Green arrows denote the interlayer displacement direction parallel (+) or antiparallel (−) to $\vec{a}$, and λ represents the interlayer displacement parameter (see text). Hollow circles '∘' mark the inversion centers in the 1T′ and T_0 phases. (d) The phonon band structure of T_0 phase shown within [-20, 80] cm^{-1}. (e) The double-well potential energy profile of T_0 phase as a function of the inversion symmetry breaking parameter λ. (f) An schematic representation showing the link between all T_d and 1T′ phases *via* the reference structure T_0.

dra are markedly distorted in the 1T′ and T_d phases [12]. Fig. 1(a,c) shows the crystal structure of $MoTe_2$ in the 1T′ and T_d phases. Both phases are quite similar, except for the fact that 1T′ is monoclinic ($\beta \neq 90$) while T_d is orthorhombic ($\alpha = \beta = \gamma = 90$). In both phases, Mo atoms dimerize forming long-short bonds along the $\vec{a}$ lattice vector and zigzag Mo-Mo metallic bonds running along the $\vec{b}$ direction.

We notice an interesting symmetry between the Mo-Te polyhedra (highlighted using light grey rectangles in Fig. 1(c)) of alternating triple layers. These polyhedra alternatively adopt either clockwise or counterclockwise twist (as viewed along $\vec{b}$) in the alternating triple layers. In the T_d phase, adjacent layers are connected by $\mathcal{M}_x\,|\{\mathcal{T}(\frac{\vec{a}}{2}(1+\lambda))\}$ symmetry operation, where $\mathcal{M}_x$ is a vertical mirror, $\mathcal{T}(\vec{a}/2)$ denotes translation by $\vec{a}/2$, and λ denotes an interlayer displacement along $\vec{a}$, as shown in Fig. 1(c). The main cause of the nonzero λ is the presence of steric interactions between Te atoms in the adjacent triple layers, which drive an in-plane shift of the alternating layers along $\vec{a}$ so as to increase the separation between these atoms. Taking the above facts into account, we define a nonpolar high-symmetry phase T_0 (space group *Pnma*) having $\lambda = 0$, as shown in Fig. 1(b).

Fig. 1(d) shows an enlarged phonon spectrum of the T_0 phase. The full phonon spectra of T_0, 1T′, and T_d phases together with all the theoretical details are given in the supplemental material (SM) [53]. We notice only two phonon instabilities in the T_0 phase: (i) an unstable optical zone center phonon mode (Γ_2^-), and (ii) a linearly-dispersing unstable phonon branch along Γ-X direction indicating an elastic instability (Γ_4^+). The first instability, Γ_2^-, breaks the inversion symmetry of the T_0 phase and corresponds to an in-plane optical vibration of the alternating triple layers. By modulating T_0 phase along Γ_2^- mode, we obtain a double-well potential energy profile with two local minima at $\lambda = \pm 0.50$ Å, as shown in Fig. 1(e). These local minima belong to the two polar variants of the T_d phase, which we refer as T_d-A and T_d-B. The interlayer displacement pattern of the alternating Mo-Te triple layers in the T_d-A and T_d-B phases is $-+-+\ldots$ and $+-+-\ldots$, respectively, thus, ensuring the orthogonality of the T_d phase.

On the other hand, the elastic instability (Γ_4^+ mode) causes a shear distortion of the unit cell, making the $\vec{a}$ and $\vec{c}$ lattice vectors nonorthogonal. By modulating the T_0 phase along the Γ_4^+ mode, we obtain a similar potential energy profile as shown in Fig. 1(e) with two local minima at cell angles $\beta = 93.6^\circ$ and $\beta = 87.4^\circ$ (see SM [53]). These two local minima mark the two ferroelastic twin phases, 1T′-I and 1T′-II, of the monoclinic 1T′ phase. The obtained value of β is in excellent agreement with previous reports [4, 10, 23, 26–29, 31–34, 36, 50]. The corresponding interlayer displacement pattern of Mo-Te triple layers in the 1T′-I and 1T′-II phases is: $++++\ldots$ and $----\ldots$, respectively. Fig. 1(f) schematically represents the connection between two polar T_d phases and two ferroelastic 1T′ phases in reference to the unstable high symmetry T_0 phase. An electron beam induced tunable reversible structural phase transition among these phases has recently been experimentally realized [12].

Due to the broken inversion symmetry requirement, the path connecting the 1T'-I and 1T'-II phases cannot access the Weyl phase. Therefore, we focus on the T_d-A → T_d-B path, investigating the subtle changes in the electronic band structure that occur there. Fig. 2(a) shows the electronic band structure of T_d-$MoTe_2$ calculated with inclusion of spin-orbit coupling (SOC). The states near the Fermi energy (E_F) are mainly composed of Mo-4*d* and Te-5*p* orbitals [54]. Without SOC, the lowest conduction band and the highest valence band

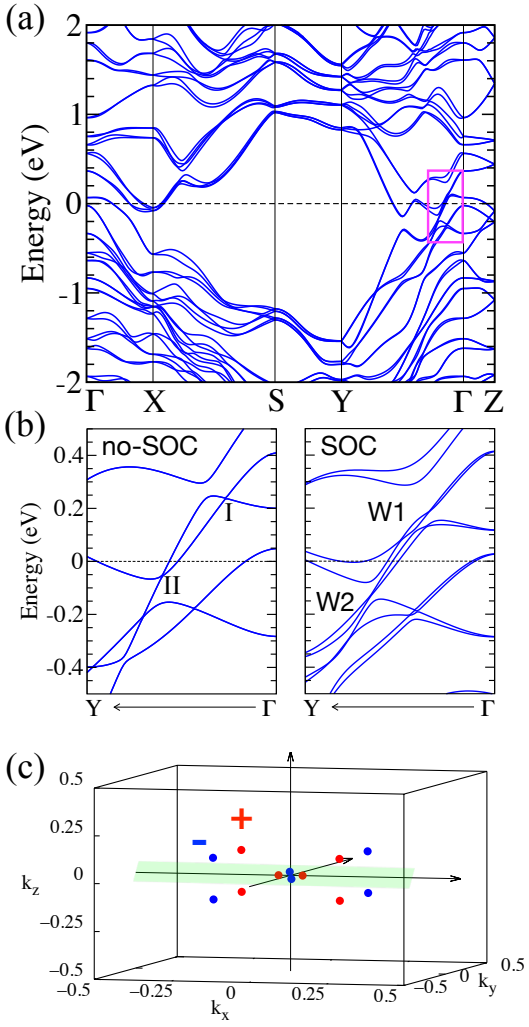

FIG. 2. (a) The electronic band structure of T_d-$MoTe_2$ calculated with-SOC. (b) An enlarged view of bands calculated without-SOC and with-SOC near the Fermi level (dotted horizontal line) along Γ-Y path, as highlighted using magenta rectangle in (a). (c) Distribution of all WPs in the BZ for T_d-A phase. Note that the chirality of WPs switches in the T_d-B phase. Red/Blue depicts WPs with +/− sign.

linearly cross each other near the Fermi level, forming type-I and type-II nodal loops above and below E_F, as marked in Fig. 2(b). Inclusion of SOC destroys the nodal loops and results in discrete gapless WPs formed slightly away from the high-symmetry directions near the Fermi level [29]. The type-I WPs (W1) are located near the Γ point (on the $k_z = 0$ plane) above the Fermi level at E_F+0.108 eV, whereas type-II WPs (W2) are located relatively farther from the Γ point (off the k_z=0 plane) at E_F−0.038 eV. A careful investigation of the electronic band structure reveals a total of 12 WPs (4 W1 and 8 W2) in the full Brillouin zone (BZ). The distribution of all 12 WPs in BZ is shown in Fig. 2(c), and their coordinates are given in the SM [53]. The T_d-A and T_d-B phases host exactly the same number of WPs at the same coordinates in momentum and energy, but with reversed chirality. This is expected since the T_d-A and T_d-B phases are related by inversion symmetry.

Motivated by the above results, we investigate the evolution of the WPs along the T_d-A → T_0 → T_d-B path as a function of λ. We observe that WPs get created in pairs as we move away from the T_d-A phase (see the SM [53]). Note that the newly created pairs of WPs are of type I. The total number of WPs increases from 12 to 16 and then 20, 24, 28, and 32, as we vary $|\lambda/\lambda_0|$ from 1.0 to 0.92, 0.88, 0.79, 0.72, and 0.63, respectively (λ_0 = 0.50 Å). The maximum number of obtained WPs is 32. This finding explains why previous authors reported such different counts of the number of Weyl points [23–26, 29, 32, 36], and reveals that the total number of WPs in $MoTe_2$ is very sensitive to the lattice distortions. As we further tune $|\lambda/\lambda_0|$, the WPs move towards their opposite partners in momentum space and start pair-annihilating, leaving no remaining WPs at $|\lambda/\lambda_0| = 0$ (at T_0 phase).

Due to the absence of WPs and the presence of a double band inversion at the Γ point, the T_0 phase turns into a second-order topological insulator, similar to the 1T′ phase [37, 38]. Notably, we find that both the T_0 and 1T′ phases belong to a strong topological class 20 as classified in Ref. [55] having topological invariant z_4=2. As we cross the T_0 phase and migrate towards the T_d-B phase, the WPs systematically start reappearing, and the aforementioned process repeats but with the switched chirality of WPs (details in the SM [53]). An animation showing the evolution of WPs as a function of $|\lambda/\lambda_0|$ is provided in the SM [53]. The pairwise creation/annihilation of WPs causes abrupt changes in the Berry curvature and Fermi-surface geometry yielding a nonzero Berry curvature dipole moment (BCDM) and, as a result, a nonlinear Hall effect in the T_d phase, as we discuss below.

In the study of the nonlinear quantum Hall effect [56], a transverse current is predicted to be generated by a harmonically oscillating electric field $E_c = \mathrm{Re}\{\mathcal{E}_c e^{i\omega t}\}$ in the absence of inversion symmetry. The response current up to second order reads $j_a = \mathrm{Re}\{j_a^0 + j_a^{2\omega} e^{2i\omega t}\}$, where a rectified current $j_a^0 = \chi_{abc}\,\mathcal{E}_b\mathcal{E}_c^*$ and a second-harmonic current $j_a^{2\omega} = \chi_{abc}\,\mathcal{E}_b\mathcal{E}_c$ depend on the nonlinear conductivity tensor χ_{abc}, where $a, b, c \in \{x, y, x\}$. The nonlinear conductivity tensor associated with the BCDM (D_{bd}) can be written as

$$\chi_{abc}(\omega) = -\varepsilon_{adc}\frac{e^3\tau}{2(1+i\omega\tau)}D_{bd}, \tag{1}$$

where ε_{abc} is the rank-three Levi-Civita symbol and τ is the relaxation time. The D_{bd} is obtained by integrating Berry curvature, weighted by the Cartesian component of the group velocity on the Fermi surface according to

$$D_{bd} = \oint_{\mathrm{FS}} \frac{d^2\boldsymbol{k}}{(2\pi)^3}\sum_n v_b^n(\boldsymbol{k})\Omega_d^n(\boldsymbol{k}), \tag{2}$$

where $v_b^n(\boldsymbol{k}) = \partial_{k_b} E_{n\boldsymbol{k}}/|\nabla_{\boldsymbol{k}} E_{n\boldsymbol{k}}|$ is a normalized group velocity component for band n, and $\boldsymbol{\Omega}^n$ is the Berry curvature pseudovector defined *via* $\Omega_{bc}^n = \varepsilon_{abc}\,\Omega_a^n$. The superscripts represent band indices. We compute the Berry curvature using the Kubo formula

$$\Omega_{ab}^n(\boldsymbol{k}) = -2\hbar^2 \sum_{m\neq n} \mathrm{Im}\frac{\langle n\boldsymbol{k}|\hat{v}_a|m\boldsymbol{k}\rangle\,\langle m\boldsymbol{k}|\hat{v}_b|n\boldsymbol{k}\rangle}{\left(E_{n\boldsymbol{k}} - E_{m\boldsymbol{k}}\right)^2 + \delta^2}, \quad (3)$$

where $\hat{v}_a$ is the velocity operator and $\delta = 0.1\,\mathrm{meV}$ is a broadening term (see [57] for numerical details).

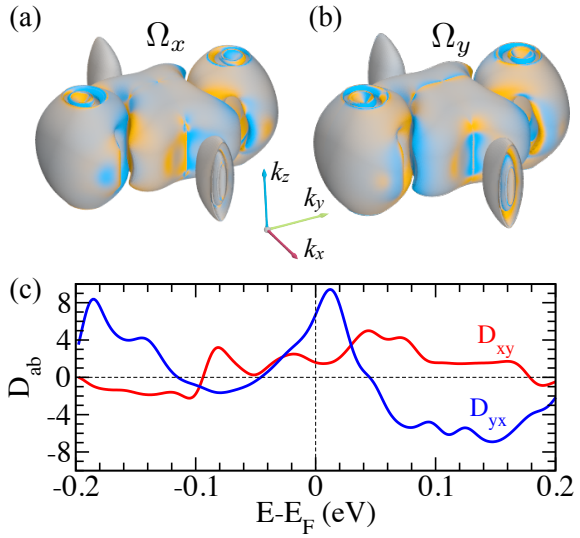

FIG. 3. Calculated Berry curvature (a) Ω_x and (b) Ω_y on the Fermi surface of $MoTe_2$ in T_d-A phase. Yellow (Blue) color represents positive (negative) Berry curvature. (c) Calculated BCDM of $MoTe_2$ in T_d-A phase. The non-vanishing D_{xy} and D_{yz} terms are plotted with respect to the chemical potential.

In the presence of inversion symmetry, i.e., the case of 1T′-$MoTe_2$, the BCDM completely vanishes. Instead, in the polar T_d phase, a non-vanishing BCDM is allowed [56, 58]. $MoTe_2$ in the T_d phase exhibits simple mirror $\mathcal{M}_y$ and glide mirror $\mathcal{M}_x\mathcal{T}(\vec{c}/2)$ symmetries, exerting constraints on the BCDM tensor. For instance, $\mathcal{M}_y$, a mirror plane normal to the chain direction, forces the group velocity v_a and Berry curvature Ω_b to obey

$$\mathcal{M}_y : (v_x, v_y, v_z) \to (v_x, -v_y, v_z) \quad (4)$$

$$(\Omega_x, \Omega_y, \Omega_z) \to (-\Omega_x, \Omega_y, -\Omega_z). \quad (5)$$

Here, the v_i denotes group velocity for a particular band at a particular $\boldsymbol{k}$. Thus, under the $\mathcal{M}_y$ symmetry operation, all components of the BCDM tensor vanish except for the D_{xy}, D_{yx}, D_{yz}, and D_{zy} terms. A further consideration of $\mathcal{M}_x\mathcal{T}(\vec{c}/2)$ symmetry eliminates the D_{yz} and D_{zy} terms as well. Thus, only two terms, D_{xy} and D_{yx}, survive in T_d-$MoTe_2$.

Fig. 3(a-b) shows the calculated Berry curvature Ω_x and Ω_y projected on the Fermi surface. The central bulb, a hole pocket at the Γ point, is pinched by two electron pockets along the k_y direction. From the Berry curvature distribution plot on the Fermi surface, one can anticipate the non-vanishing nature of the D_{xy} and D_{yx} terms. Because of the complex metallic bands with anisotropic group velocities in type-II Weyl semimetals, the Fermi surface has significant Berry curvature even away from the WPs (see the SM [53]). This renders the BCDM more sensitive to the chemical potential than for type-I Weyl semimetals [21, 59]. In the latter, the major contribution to the BCDM comes from the WPs, whereas the rest of the Fermi surface makes a negligible contribution due to the isotropic group velocities near the WPs. Therefore, we notice a considerable change in the BCDM with respect to the chemical potential in T_d-$MoTe_2$.

The nonvanishing D_{xy} and D_{yx} terms in the T_d-A phase, computed as a function of the chemical potential, are shown in Fig. 3(c). D_{yx} is peaked near the Fermi level, while D_{xy} exhibits oscillating behavior. (Note that the BCDM is a dimensionless quantity in three dimensions.) At E_F, D_{xy} and D_{yx} are estimated to be 1.6 and 6.7, respectively. These values are several times larger than the corresponding $D_{xy} = 0.8$ and $D_{yx} = -0.7$ reported for T_d-$MoTe_2$ by Zhang et al. [21]. The main reason behind this difference is the strong sensitivity of the Fermi surface to the on-site Hubbard U of Mo $4d$ electrons [25, 36], which was not taken into account in the previous study [21]. Indeed, only four WPs are reported in their study, in contrast to the twelve (8 type-II and 4 type-I) obtained in our case.

From Eq. 1, the nonlinear conductivity tensor has nonzero terms $\chi_{xxz} = -\chi_{zxx}$ associated with D_{xy}, and $\chi_{zyy} = -\chi_{yyz}$ associated with D_{yx}. In view of the significant peak in D_{yx} near E_F, one interesting measurement would be the observation of a transverse current j_z induced by an oscillating electric field along y direction. In the $\omega \to 0$ limit, an external electric field applied along the y direction, i.e., the chain direction, generates an out-of-plane current $j_z^0 = 2\chi_{zyy}|\mathcal{E}_y|^2$. If one can raise the electron chemical potential *via* gating, the transverse current j_z^0 is predicted to rapidly reach its maximum and then decrease, and eventually reverse its sign.

Here, we stress that a structural transition from the T_d-A to T_d-B phase flips the sign of D_{ab} while keeping its magnitude intact, thus, allowing one to distinguish between the two variants of polar T_d phases. For this purpose, observation of D_{xy} via $j_z^0 = 2\chi_{zxx}|\mathcal{E}_x|^2$ may be most suitable, since the sign of D_{xy} is less sensitive to the electron chemical potential. We do not notice significant differences in the magnitudes of D_{ab} for the intermediate structures along the polarity reversal path, although new pairs of WPs get created/annihilated as a function of λ. This is due to the fact that the newly created WPs belong to the type-I category which have relatively smaller tilt of Weyl cone compared to type-II category, thus yielding minimal changes to the overall BCDM.

An interesting aspect of the nonlinear Hall conductivity in this system is that, because the surfaces have lower symmetry than the bulk, new components of the D tensor are activated at the surface. In particular, the glide mirror $\mathcal{M}_x\,\mathcal{T}(\vec{c}/2)$ is broken at the (001) cleavage surface. Recall that the D_{yz} and D_{zy} tensor elements were argued to vanish in the bulk because of this glide mirror, but they need not vanish at the surface. Thus, response currents associated with the conductivity tensor elements $\chi_{yyx} = -\chi_{xyy}$ and $\chi_{xzz} = -\chi_{zzx}$ are allowed. While we can confidently predict the existence of such currents, we are not currently in a position to compute the surface D tensors quantitatively. This observation thus provides a challenge for future efforts at both theoretical prediction and experimental detection of surface nonlinear Hall responses.

We may also consider the symmetries that remain in the exfoliated single-layer limit. In fact, the $\chi_{yyx} = -\chi_{xyy} \propto D_{yz}$ tensor elements are the only ones to survive in this limit. The other terms, proportional to Ω_x or Ω_y, are not well defined in two dimensions. Therefore, measuring the in-plane nonlinear Hall conductivity of $MoTe_2$ with respect to the film thickness may reveal a noticeable transition from the film to the surface responses.

In principle, one can utilize the nonlinear response current generated due to the rapid fluctuation of D_{yx} and its sign reversal near the Fermi level as a function of the chemical potential to devise a nonlinear Hall transistor for practical applications. Moreover, recent experiments [41, 60] demonstrated an ultrafast optical control over T_d and $1T'$ structural phase transitions, hence, an ultrafast topological optical switch can be designed using the nonlinear quantum Hall property of $MoTe_2$, where T_d ($1T'$) phase can act as an ON (OFF) state.

In summary, we explain the intricate structural phase transitions in $MoTe_2$ by defining a high-symmetry nonpolar phase T_0 that exhibits a higher-order topology. We unveil the connection between the Weyl phase and the higher-order topological phase in $MoTe_2$. We report that WPs can be readily created/annihilated, manipulated, and switched by controlling the structural phase transitions between the two polar variants of the T_d phase. Since this structural phase switching has already been experimentally achieved, and is shown to be reversible [12], $MoTe_2$ offers a promising platform to harness the dynamics of Weyl fermions for technological applications. We also report on the presence of a tunable nonlinear Hall effect in T_d-$MoTe_2$, and discuss the potential applications of this effect in designing ultrafast topological optical switches and transistors. We further predict that an emergent nonlinear surface response current, arising solely due to the surface effects, can be observed in a slab geometry. One can quantify the magnitude of the emergent surface response current by reducing the dimensionality of the system. The synergy between the possible experimental control over the atomic arrangements, Weyl phase, and the nonlinear quantum Hall effects in $MoTe_2$ paves the way for realization of Weyltronics.

We thank Fei-ting Huang and Sang-Wook Cheong for fruitful discussions. The work was supported by ONR Grants N00014-16-1-2951 and N00014-17-1-2449.

Note: Supplemental Materials can be obtained from the corresponding author on reasonable request.

* sobhit.singh@rutgers.edu

[1] Qing Hua Wang, Kourosh Kalantar-Zadeh, Andras Kis, Jonathan N. Coleman, and Michael S. Strano, "Electronics and optoelectronics of two-dimensional transition metal dichalcogenides," Nature Nanotechnology **7**, 699 (2012).

[2] Dong Hoon Keum, Suyeon Cho, Jung Ho Kim, Duk-Hyun Choe, Ha-Jun Sung, Min Kan, Haeyong Kang, Jae-Yeol Hwang, Sung Wng Kim, Heejun Yang, K. J. Chang, and Young Hee Lee, "Bandgap opening in few-layered monoclinic $MoTe_2$," Nature Physics **11**, 482–486 (2015).

[3] Kenan Zhang, Changhua Bao, Qiangqiang Gu, Xiao Ren, Haoxiong Zhang, Ke Deng, Yang Wu, Yuan Li, Ji Feng, and Shuyun Zhou, "Raman signatures of inversion symmetry breaking and structural phase transition in type-II Weyl semimetal $MoTe_2$," Nature Communications **7**, 13552 (2016).

[4] Hyun-Jung Kim, Seoung-Hun Kang, Ikutaro Hamada, and Young-Woo Son, "Origins of the structural phase transitions in $MoTe_2$ and WTe_2," Phys. Rev. B **95**, 180101 (2017).

[5] Ying Wang, Jun Xiao, Hanyu Zhu, Yao Li, Yousif Alsaid, King Yan Fong, Yao Zhou, Siqi Wang, Wu Shi, Yuan Wang, Alex Zettl, Evan J. Reed, and Xiang Zhang, "Structural phase transition in monolayer $MoTe_2$ driven by electrostatic doping," Nature **550**, 487–491 (2017).

[6] Gang Wang, Alexey Chernikov, Mikhail M. Glazov, Tony F. Heinz, Xavier Marie, Thierry Amand, and Bernhard Urbaszek, "Colloquium: Excitons in atomically thin transition metal dichalcogenides," Rev. Mod. Phys. **90**, 021001 (2018).

[7] Ayelet Notis Berger, Erick Andrade, Alexander Kerelsky, Drew Edelberg, Jian Li, Zhijun Wang, Lunyong Zhang, Jaewook Kim, Nader Zaki, Jose Avila, Chaoyu Chen, Maria C. Asensio, Sang-Wook Cheong, Bogdan A. Bernevig, and Abhay N. Pasupathy, "Temperature-driven topological transition in $1T'$-$MoTe_2$," npj Quantum Materials **3**, 2 (2018).

[8] Wencan Jin, Theanne Schiros, Yi Lin, Junzhang Ma, Rui Lou, Zhongwei Dai, Jie-Xiang Yu, Daniel Rhodes, Jerzy T. Sadowski, Xiao Tong, Tian Qian, Makoto Hashimoto, Donghui Lu, Jerry I. Dadap, Shancai Wang, Elton J. G. Santos, Jiadong Zang, Karsten Pohl, Hong Ding, James Hone, Luis Balicas, Abhay N. Pasupathy, and Richard M. Osgood, "Phase transition and electronic structure evolution of $MoTe_2$ induced by W substitution," Phys. Rev. B **98**, 144114 (2018).

[9] Chen Si, Dukhyun Choe, Weiyu Xie, Han Wang, Zhimei Sun, Junhyeok Bang, and Shengbai Zhang, "Photoinduced vacancy ordering and phase transition in $MoTe_2$,"

Nano Letters, Nano Letters **19**, 3612–3617 (2019).
[10] Colin Heikes, I-Lin Liu, Tristin Metz, Chris Eckberg, Paul Neves, Yan Wu, Linda Hung, Phil Piccoli, Huibo Cao, Juscelino Leao, Johnpierre Paglione, Taner Yildirim, Nicholas P. Butch, and William Ratcliff, "Mechanical control of crystal symmetry and superconductivity in Weyl semimetal $MoTe_2$," Phys. Rev. Materials **2**, 074202 (2018).
[11] Shuoguo Yuan, Xin Luo, Hung Lit Chan, Chengcheng Xiao, Yawei Dai, Maohai Xie, and Jianhua Hao, "Room-temperature ferroelectricity in $MoTe_2$ down to the atomic monolayer limit," Nature Communications **10**, 1775 (2019).
[12] Fei-Ting Huang, Seong Joon Lim, Sobhit Singh, Jinwoong Kim, Lunyong Zhang, Jae-Wook Kim, Ming-Wen Chu, Karin M. Rabe, David Vanderbilt, and Sang-Wook Cheong, "Polar and phase domain walls with conducting interfacial states in a Weyl semimetal $MoTe_2$," Nature Communications **10**, 4211 (2019).
[13] F. C. Chen, H. Y. Lv, X. Luo, W. J. Lu, Q. L. Pei, G. T. Lin, Y. Y. Han, X. B. Zhu, W. H. Song, and Y. P. Sun, "Extremely large magnetoresistance in the type-II Weyl semimetal $MoTe_2$," Phys. Rev. B **94**, 235154 (2016).
[14] Q. L. Pei, W. J. Meng, X. Luo, H. Y. Lv, F. C. Chen, W. J. Lu, Y. Y. Han, P. Tong, W. H. Song, Y. B. Hou, Q. Y. Lu, and Y. P. Sun, "Origin of the turn-on phenomenon in T_d-MoTe_2," Phys. Rev. B **96**, 075132 (2017).
[15] S. Thirupathaiah, Rajveer Jha, Banabir Pal, J. S. Matias, P. Kumar Das, P. K. Sivakumar, I. Vobornik, N. C. Plumb, M. Shi, R. A. Ribeiro, and D. D. Sarma, "$MoTe_2$: An uncompensated semimetal with extremely large magnetoresistance," Phys. Rev. B **95**, 241105 (2017).
[16] Sangyun Lee, Jaekyung Jang, Sung-Il Kim, Soon-Gil Jung, Jihyun Kim, Suyeon Cho, Sung Wng Kim, Joo Yull Rhee, Kee-Su Park, and Tuson Park, "Origin of extremely large magnetoresistance in the candidate type-II Weyl semimetal $MoTe_2$," Scientific Reports **8**, 13937 (2018).
[17] F. C. Chen, X. Luo, J. Yan, Y. Sun, H. Y. Lv, W. J. Lu, C. Y. Xi, P. Tong, Z. G. Sheng, X. B. Zhu, W. H. Song, and Y. P. Sun, "Planar Hall effect in the type-II Weyl semimetal T_d-MoTe_2," Phys. Rev. B **98**, 041114 (2018).
[18] Yang Zhang, Jeroen van den Brink, Claudia Felser, and Binghai Yan, "Electrically tuneable nonlinear anomalous Hall effect in two-dimensional transition-metal dichalcogenides WTe_2 and $MoTe_2$," 2D Materials **5**, 044001 (2018).
[19] Xiaofeng Qian, Junwei Liu, Liang Fu, and Ju Li, "Quantum spin Hall effect in two-dimensional transition metal dichalcogenides," Science **346**, 1344–1347 (2014).
[20] Sejoon Lim, Catherine R. Rajamathi, Vicky Süß, Claudia Felser, and Aharon Kapitulnik, "Temperature-induced inversion of the spin-photogalvanic effect in WTe_2 and $MoTe_2$," Phys. Rev. B **98**, 121301 (2018).
[21] Yang Zhang, Yan Sun, and Binghai Yan, "Berry curvature dipole in Weyl semimetal materials: An ab initio study," Phys. Rev. B **97**, 041101 (2018).
[22] Jiaqi Zhou, Junfeng Qiao, Arnaud Bournel, and Weisheng Zhao, "Intrinsic spin Hall conductivity of the semimetals $MoTe_2$ and WTe_2," Phys. Rev. B **99**, 060408 (2019).
[23] D. Rhodes, R. Schönemann, N. Aryal, Q. Zhou, Q. R. Zhang, E. Kampert, Y.-C. Chiu, Y. Lai, Y. Shimura, G. T. McCandless, J. Y. Chan, D. W. Paley, J. Lee, A. D. Finke, J. P. C. Ruff, S. Das, E. Manousakis, and L. Balicas, "Bulk Fermi surface of the Weyl type-II semimetallic candidate $\gamma-MoTe_2$," Phys. Rev. B **96**, 165134 (2017).
[24] Andrew P. Weber, Philipp Rüßmann, Nan Xu, Stefan Muff, Mauro Fanciulli, Arnaud Magrez, Philippe Bugnon, Helmuth Berger, Nicholas C. Plumb, Ming Shi, Stefan Blügel, Phivos Mavropoulos, and J. Hugo Dil, "Spin-resolved electronic response to the phase transition in $MoTe_2$," Phys. Rev. Lett. **121**, 156401 (2018).
[25] Niraj Aryal and Efstratios Manousakis, "Importance of electron correlations in understanding photoelectron spectroscopy and Weyl character of $MoTe_2$," Phys. Rev. B **99**, 035123 (2019).
[26] Yan Sun, Shu-Chun Wu, Mazhar N. Ali, Claudia Felser, and Binghai Yan, "Prediction of Weyl semimetal in orthorhombic $MoTe_2$," Phys. Rev. B **92**, 161107 (2015).
[27] Alexey A. Soluyanov, Dominik Gresch, Zhijun Wang, QuanSheng Wu, Matthias Troyer, Xi Dai, and B. Andrei Bernevig, "Type-II Weyl semimetals," Nature **527**, 495 (2015).
[28] Lunan Huang, Timothy M. McCormick, Masayuki Ochi, Zhiying Zhao, Michi-To Suzuki, Ryotaro Arita, Yun Wu, Daixiang Mou, Huibo Cao, Jiaqiang Yan, Nandini Trivedi, and Adam Kaminski, "Spectroscopic evidence for a type II Weyl semimetallic state in $MoTe_2$," Nature Materials **15**, 1155 (2016).
[29] Zhijun Wang, Dominik Gresch, Alexey A. Soluyanov, Weiwei Xie, S. Kushwaha, Xi Dai, Matthias Troyer, Robert J. Cava, and B. Andrei Bernevig, "$MoTe_2$: A type-II Weyl topological metal," Phys. Rev. Lett. **117**, 056805 (2016).
[30] Ke Deng, Guoliang Wan, Peng Deng, Kenan Zhang, Shijie Ding, Eryin Wang, Mingzhe Yan, Huaqing Huang, Hongyun Zhang, Zhilin Xu, Jonathan Denlinger, Alexei Fedorov, Haitao Yang, Wenhui Duan, Hong Yao, Yang Wu, Shoushan Fan, Haijun Zhang, Xi Chen, and Shuyun Zhou, "Experimental observation of topological Fermi arcs in type-II Weyl semimetal $MoTe_2$," Nature Physics **12**, 1105–1110 (2016).
[31] A. Tamai, Q. S. Wu, I. Cucchi, F. Y. Bruno, S. Riccò, T. K. Kim, M. Hoesch, C. Barreteau, E. Giannini, C. Besnard, A. A. Soluyanov, and F. Baumberger, "Fermi arcs and their topological character in the candidate type-II Weyl semimetal $MoTe_2$," Phys. Rev. X **6**, 031021 (2016).
[32] A. Crepaldi, G. Autès, G. Gatti, S. Roth, A. Sterzi, G. Manzoni, M. Zacchigna, C. Cacho, R. T. Chapman, E. Springate, E. A. Seddon, Ph. Bugnon, A. Magrez, H. Berger, I. Vobornik, M. Kalläne, A. Quer, K. Rossnagel, F. Parmigiani, O. V. Yazyev, and M. Grioni, "Enhanced ultrafast relaxation rate in the Weyl semimetal phase of $MoTe_2$ measured by time- and angle-resolved photoelectron spectroscopy," Phys. Rev. B **96**, 241408 (2017).
[33] H. Takahashi, T. Akiba, K. Imura, T. Shiino, K. Deguchi, N. K. Sato, H. Sakai, M. S. Bahramy, and S. Ishiwata, "Anticorrelation between polar lattice instability and superconductivity in the Weyl semimetal candidate $MoTe_2$," Phys. Rev. B **95**, 100501 (2017).
[34] Yanpeng Qi, Pavel G. Naumov, Mazhar N. Ali, Catherine R. Rajamathi, Walter Schnelle, Oleg Barkalov, Michael Hanfland, Shu-Chun Wu, Chandra Shekhar, Yan

Sun, Vicky Süß, Marcus Schmidt, Ulrich Schwarz, Eckhard Pippel, Peter Werner, Reinald Hillebrand, Tobias Förster, Erik Kampert, Stuart Parkin, R. J. Cava, Claudia Felser, Binghai Yan, and Sergey A. Medvedev, "Superconductivity in Weyl semimetal candidate $MoTe_2$," Nature Communications **7**, 11038 (2016).

[35] Anmin Zhang, Xiaoli Ma, Changle Liu, Rui Lou, Yimeng Wang, Qiaohe Yu, Yiyan Wang, Tian-long Xia, Shancai Wang, Lei Zhang, Xiaoqun Wang, Changfeng Chen, and Qingming Zhang, "Topological phase transition between distinct Weyl semimetal states in $MoTe_2$," Phys. Rev. B **100**, 201107 (2019).

[36] N. Xu, Z. W. Wang, A. Magrez, P. Bugnon, H. Berger, C. E. Matt, V. N. Strocov, N. C. Plumb, M. Radovic, E. Pomjakushina, K. Conder, J. H. Dil, J. Mesot, R. Yu, H. Ding, and M. Shi, "Evidence of a Coulomb-interaction-induced Lifshitz transition and robust hybrid Weyl semimetal in T_d−$MoTe_2$," Phys. Rev. Lett. **121**, 136401 (2018).

[37] Zhijun Wang, Benjamin J. Wieder, Jian Li, Binghai Yan, and B. Andrei Bernevig, "Higher-order topology, monopole nodal lines, and the origin of large fermi arcs in transition metal dichalcogenides XTe_2 (X = Mo, W)," Phys. Rev. Lett. **123**, 186401 (2019).

[38] Feng Tang, Hoi Chun Po, Ashvin Vishwanath, and Xiangang Wan, "Efficient topological materials discovery using symmetry indicators," Nature Physics **15**, 470–476 (2019).

[39] Motohiko Ezawa, "Second-order topological insulators and loop-nodal semimetals in transition metal dichalcogenides XTe_2 (X = Mo, W)," Scientific Reports **9**, 5286 (2019).

[40] Shao-Yu Chen, Thomas Goldstein, Dhandapani Venkataraman, Ashwin Ramasubramaniam, and Jun Yan, "Activation of new Raman modes by inversion symmetry breaking in type II Weyl semimetal candidate T′-$MoTe_2$," *Nano Letters*, Nano Letters **16**, 5852–5860 (2016).

[41] M. Y. Zhang, Z. X. Wang, Y. N. Li, L. Y. Shi, D. Wu, T. Lin, S. J. Zhang, Y. Q. Liu, Q. M. Liu, J. Wang, T. Dong, and N. L. Wang, "Light-induced subpicosecond lattice symmetry switch in $MoTe_2$," Phys. Rev. X **9**, 021036 (2019).

[42] Rui He, Shazhou Zhong, Hyun Ho Kim, Gaihua Ye, Zhipeng Ye, Logan Winford, Daniel McHaffie, Ivana Rilak, Fangchu Chen, Xuan Luo, Yuping Sun, and Adam W. Tsen, "Dimensionality-driven orthorhombic $MoTe_2$ at room temperature," Phys. Rev. B **97**, 041410 (2018).

[43] Polychronis Tsipas, Sotirios Fragkos, Dimitra Tsoutsou, Carlos Alvarez, Roberto Sant, Gilles Renaud, Hanako Okuno, and Athanasios Dimoulas, "Direct observation at room temperature of the orthorhombic Weyl semimetal phase in thin epitaxial $MoTe_2$," Advanced Functional Materials **28**, 1802084 (2018).

[44] Xue-Jun Yan, Yang-Yang Lv, Lei Li, Xiao Li, Shu-Hua Yao, Yan-Bin Chen, Xiao-Ping Liu, Hong Lu, Ming-Hui Lu, and Yan-Feng Chen, "Investigation on the phase-transition-induced hysteresis in the thermal transport along the c-axis of $MoTe_2$," npj Quantum Materials **2**, 31 (2017).

[45] Yu Tao, John A. Schneeloch, Chunruo Duan, Masaaki Matsuda, Sachith E. Dissanayake, Adam A. Aczel, Jaime A. Fernandez-Baca, Feng Ye, and Despina Louca, "Appearance of a T_d^* phase across the $T_d - 1T^{'}$ phase boundary in the Weyl semimetal $MoTe_2$," Phys. Rev. B **100**, 100101 (2019).

[46] Sachith Dissanayake, Chunruo Duan, Junjie Yang, Jun Liu, Masaaki Matsuda, Changming Yue, John A. Schneeloch, Jeffrey C. Y. Teo, and Despina Louca, "Electronic band tuning under pressure in $MoTe_2$ topological semimetal," npj Quantum Materials **4**, 45 (2019).

[47] Su-Yang Xu, Qiong Ma, Huitao Shen, Valla Fatemi, Sanfeng Wu, Tay-Rong Chang, Guoqing Chang, Andrés M. Mier Valdivia, Ching-Kit Chan, Quinn D. Gibson, Jiadong Zhou, Zheng Liu, Kenji Watanabe, Takashi Taniguchi, Hsin Lin, Robert J. Cava, Liang Fu, Nuh Gedik, and Pablo Jarillo-Herrero, "Electrically switchable Berry curvature dipole in the monolayer topological insulator WTe_2," Nature Physics **14**, 900–906 (2018).

[48] T. Ideue, K. Hamamoto, S. Koshikawa, M. Ezawa, S. Shimizu, Y. Kaneko, Y. Tokura, N. Nagaosa, and Y. Iwasa, "Bulk rectification effect in a polar semiconductor," Nature Physics **13**, 578 (2017).

[49] D. N. Basov, M. M. Fogler, and F. J. García de Abajo, "Polaritons in van der Waals materials," Science **354** (2016).

[50] R. Clarke, E. Marseglia, and H. P. Hughes, "A low-temperature structural phase transition in β-$MoTe_2$," Philosophical Magazine B **38**, 121–126 (1978).

[51] Xiaoli Ma, Pengjie Guo, Changjiang Yi, Qiaohe Yu, Anmin Zhang, Jianting Ji, Yong Tian, Feng Jin, Yiyan Wang, Kai Liu, Tianlong Xia, Youguo Shi, and Qingming Zhang, "Raman scattering in the transition-metal dichalcogenides of $1T^{'}$−$MoTe_2$, T_d−$MoTe_2$, and T_d−WTe_2," Phys. Rev. B **94**, 214105 (2016).

[52] John A. Schneeloch, Chunruo Duan, Junjie Yang, Jun Liu, Xiaoping Wang, and Despina Louca, "Emergence of topologically protected states in the $MoTe_2$ Weyl semimetal with layer-stacking order," Phys. Rev. B **99**, 161105 (2019).

[53] "See Supplemental Material (SM) at href for numerical details, and for additional information regarding the calculated phonon spectrum, potential energy barrier profile for 1T′ twin phases, electronic bandstructure, evolution of WPs and BCDM as a function of λ, coordinates of all WPs, higher-order topological classification of T_0 and 1T′ phases. SM comprises Refs. [7, 25, 36, 37, 40, 44, 50, 55, 61–70]".

[54] Due to the semicorrelated nature of Mo-4d orbitals, pure DFT fails to correctly describe the Angle-Resolved Photoemission Spectroscopy (ARPES) data and pressure dependence of quantum oscillation frequency measurements in $MoTe_2$ [25, 36, 71]. Adding an on-site Hubbard term (U_{eff}), the Hubbard term, on Mo-4d orbitals has been reported to solve this issue. Therefore, we consider $U_{\text{eff}} = 2.4\,\text{eV}$ as suggested by Xu et al. [36].

[55] M. G. Vergniory, L. Elcoro, Claudia Felser, Nicolas Regnault, B. Andrei Bernevig, and Zhijun Wang, "A complete catalogue of high-quality topological materials," Nature **566**, 480–485 (2019).

[56] Inti Sodemann and Liang Fu, "Quantum nonlinear Hall effect induced by Berry curvature dipole in time-reversal invariant materials," Phys. Rev. Lett. **115**, 216806 (2015).

[57] Due to the heavy computational cost of the Kubo formula and slow convergence of BCDM with respect to the

k-mesh size, we first compute the Fermi surface by employing the tetrahedron method at a given k-grid, and sample Berry curvature only at the reduced grid points near the Fermi surface. The convergence of BCDM was achieved at a k-grid of size $278 \times 510 \times 130$ with Gaussian smearing, where the broadening width corresponds to $\sim$50 K.

[58] Qiong Ma, Su-Yang Xu, Huitao Shen, David MacNeill, Valla Fatemi, Tay-Rong Chang, Andrés M. Mier Valdivia, Sanfeng Wu, Zongzheng Du, Chuang-Han Hsu, Shiang Fang, Quinn D. Gibson, Kenji Watanabe, Takashi Taniguchi, Robert J. Cava, Efthimios Kaxiras, Hai-Zhou Lu, Hsin Lin, Liang Fu, Nuh Gedik, and Pablo Jarillo-Herrero, "Observation of the nonlinear Hall effect under time-reversal-symmetric conditions," Nature **565**, 337–342 (2019).

[59] Jorge I. Facio, Dmitri Efremov, Klaus Koepernik, Jhih-Shih You, Inti Sodemann, and Jeroen van den Brink, "Strongly enhanced Berry dipole at topological phase transitions in bitei," Phys. Rev. Lett. **121**, 246403 (2018).

[60] Edbert J. Sie, Clara M. Nyby, C. D. Pemmaraju, Su Ji Park, Xiaozhe Shen, Jie Yang, Matthias C. Hoffmann, B. K. Ofori-Okai, Renkai Li, Alexander H. Reid, Stephen Weathersby, Ehren Mannebach, Nathan Finney, Daniel Rhodes, Daniel Chenet, Abhinandan Antony, Luis Balicas, James Hone, Thomas P. Devereaux, Tony F. Heinz, Xijie Wang, and Aaron M. Lindenberg, "An ultrafast symmetry switch in a Weyl semimetal," Nature **565**, 61–66 (2019).

[61] G. Kresse and J. Furthmüller, "Efficient iterative schemes for ab initio total-energy calculations using a plane-wave basis set," Phys. Rev. B **54**, 11169–11186 (1996).

[62] G. Kresse and J. Furthmüller, "Efficiency of ab-initio total energy calculations for metals and semiconductors using a plane-wave basis set," Computational Materials Science **6**, 15 – 50 (1996).

[63] P. E. Blöchl, "Projector augmented-wave method," Phys. Rev. B **50**, 17953–17979 (1994).

[64] G. Kresse and D. Joubert, "From ultrasoft pseudopotentials to the projector augmented-wave method," Phys. Rev. B **59**, 1758–1775 (1999).

[65] John P. Perdew, Adrienn Ruzsinszky, Gábor I. Csonka, Oleg A. Vydrov, Gustavo E. Scuseria, Lucian A. Constantin, Xiaolan Zhou, and Kieron Burke, "Restoring the density-gradient expansion for exchange in solids and surfaces," Phys. Rev. Lett. **100**, 136406 (2008).

[66] S. L. Dudarev, G. A. Botton, S. Y. Savrasov, C. J. Humphreys, and A. P. Sutton, "Electron-energy-loss spectra and the structural stability of nickel oxide: An LSDA+U study," Phys. Rev. B **57**, 1505–1509 (1998).

[67] Sobhit Singh, Irais Valencia-Jaime, Olivia Pavlic, and Aldo H. Romero, "Elastic, mechanical, and thermodynamic properties of Bi-Sb binaries: Effect of spin-orbit coupling," Phys. Rev. B **97**, 054108 (2018).

[68] A Togo and I Tanaka, "First principles phonon calculations in materials science," Scr. Mater. **108**, 1–5 (2015).

[69] QuanSheng Wu, ShengNan Zhang, Hai-Feng Song, Matthias Troyer, and Alexey A. Soluyanov, "Wanniertools: An open-source software package for novel topological materials," Computer Physics Communications **224**, 405 – 416 (2018).

[70] Uthpala Herath, Pedram Tavadze, Xu He, Eric Bousquet, Sobhit Singh, Francisco Muoz, and Aldo H. Romero, "Pyprocar: A Python library for electronic structure pre/post-processing," Computer Physics Communications , 107080 (2019).

[71] Shin-ichi Kimura, Yuki Nakajima, Zenjiro Mita, Rajveer Jha, Ryuji Higashinaka, Tatsuma D. Matsuda, and Yuji Aoki, "Optical evidence of the type-II Weyl semimetals $MoTe_2$ and WTe_2," Phys. Rev. B **99**, 195203 (2019).